Original properties of dipole vortices in zero-dimensional ferroelectrics

2008 J. Phys.: Condens. Matter 20 193201

(http://iopscience.iop.org/0953-8984/20/19/193201)

IOP PUBLISHING JOURNAL OF PHYSICS: CONDENSED MATTER

J. Phys.: Condens. Matter **20** (2008) 193201 (14pp) doi:10.1088/0953-8984/20/19/193201

TOPICAL REVIEW

Original properties of dipole vortices in zero-dimensional ferroelectrics

S Prosandeev[1,2], I Ponomareva[1], I Naumov[1,3], I Kornev[1,4] and L Bellaiche[1]

[1] Physics Department, University of Arkansas, Fayetteville, AR 72701, USA
[2] Research Institute of Physics, Southern Federal University, 344090 Rostov on Don, Russia
[3] Hewlett-Packard Information and Quantum Systems Laboratory, 1501 Page Mill Road, Palo Alto, CA 94304, USA
[4] Mads Clausen Institute for Product Innovation, University of Southern Denmark, Alsion 2, DK-6400 Sønderborg, Denmark

Received 3 January 2008, in final form 27 February 2008
Published 8 April 2008
Online at stacks.iop.org/JPhysCM/20/193201

Abstract
The very recent use of first-principles-based simulations to investigate zero-dimensional ferroelectrics has led to the discovery of electric vortices, as well as of many original properties associated with these vortices. These original properties are of fundamental importance and of high technological promise, and are reviewed here.

(Some figures in this article are in colour only in the electronic version)

Contents

1. Introduction

Dipole vortices in zero-dimensional *magnets* have attracted a lot of attention in the last seven years, and are being intensively studied both experimentally and theoretically by many different groups for fundamental and technological reasons (see, e.g., [1–6] and references therein). Such a situation contrasts with that occurring in another kind of dipolar nanostructures, namely zero-dimensional *ferroelectrics*. As a matter of fact, it is only four years ago that first-principles-based calculations predicted the existence of dipolar vortex structures in nanoferroelectrics [7, 8], and we are still awaiting the experimental confirmation of such fascinating structures (note, though, that major steps towards the experimental discovery of dipole vortices in ferroelectrics have been accomplished in the last two years [9, 10], which suggests that such discovery may occur rather soon). Similarly, only a few theoretical studies have been aimed to predict *properties* associated with dipolar vortices in nanoferroelectrics or, equivalently, the consequences of the existence of such vortices [7, 8, 11–17]. One major reason for this scarcity is that one needs a simulation tool able to accurately predict properties of ferroelectric nanostructures, which is quite a challenge.

The aims of this review are to discuss some of these recent studies and their predictions [7, 8, 11–17], as well as to describe the numerical method that allowed these predictions. This review is organized as follows: section 2 provides details about the effective Hamiltonian method that has been developed and/or used in these studies; section 3 describes the

morphology of dipole vortices in isolated nanoferroelectrics, and its dependence on the size and shape of the nanoparticle, the material from which the nanoparticle is made of, and its electrical boundary conditions; section 4 emphasizes the need for introducing an original order parameter to describe such vortices, namely the electric toroidal moment; section 5 is devoted to unique strain characteristics associated with dipole vortices; sections 6 and 7 deal with the existence of novel tensors resulting from the coupling of the electric toroidal moment with other physical quantities; section 8 describes an original path connecting the vortex and polarized states; section 9 is about the control of the chirality of the dipole vortices; section 10 discusses novel phases occurring in an array of ferroelectric dots embedded into a polar matrix; finally, section 11 concludes this review.

2. Effective Hamiltonian approach for zero-dimensional ferroelectrics

Stress-free zero-dimensional ferroelectrics made of disordered $PbZr_{1-x}Ti_xO_3$ (PZTx) systems, being Pb–O terminated at all surfaces, were studied. Stress-free zero-dimensional ferroelectrics made of $BaTiO_3$ (BT), being Ba–O terminated at all surfaces, were also investigated, for the sake of comparison with PZTx zero-dimensional ferroelectrics. The total energy of such systems was written as

$$\mathcal{E}_{\rm tot}(\mathbf{u}_i, \mathbf{v}_i, \eta_{\rm H}) = \mathcal{E}_{\rm Heff}(\mathbf{u}_i, \mathbf{v}_i, \eta_{\rm H}) + \tfrac{1}{2}\beta \sum_i \langle \mathbf{E}_{\rm dep} \rangle \cdot Z^* \mathbf{u}_i - \sum_i \mathbf{E} \cdot Z^* \mathbf{u}_i - a^3 \sum_j \sigma_j \eta_{{\rm H},j} \quad (1)$$

where $\mathbf{u_i}$ is the local soft mode in the unit cell i of the zero-dimensional ferroelectric—whose product with the effective charge Z^* yields the local electrical dipole, $\{\mathbf{p}_i\}$, in this cell; $\eta_{\rm H}$ is the homogeneous strain tensor (that characterizes the average elastic deformations of the whole system); $\mathbf{v}_i$ are the inhomogeneous strain-related (acoustic-type) displacements in unit cell i, which describe the remaining (that is, after subtraction of the homogeneous part) elastic deformations inside the system [18]. Here, the six components of $\eta_{\rm H}$ in Voigt notation [19] are denoted as $\eta_{{\rm H},j}$, where j can run from 1 to 6.

$\mathcal{E}_{\rm Heff}$ represents the intrinsic (effective Hamiltonian) energy of zero-dimensional ferroelectrics. Its analytical expression is that of [18] for BT bulk and of [20] for PZTx bulk (while its first-principles-derived parameters are those of [21] for BT and of [20] for PZTx), except for two main modifications. The first modification consists in adding energetic terms associated with the direct interaction between the vacuum surrounding the zero-dimensional ferroelectric and both the surface dipoles and inhomogeneous strain near the surface [7, 22]. The second modification consists in replacing the (reciprocal-space-based) matrix associated with long-range dipole–dipole interactions in the bulk [18] by the corresponding (real-space-based) matrix characterizing dipole–dipole interactions in the zero-dimensional ferroelectric—implying that no supercell periodic boundary conditions are needed to simulate the zero-dimensional ferroelectric. Such a matrix is given in [11, 23] and corresponds to ideal open-circuit (OC) conditions, for which no possible screening of the polarization-induced surface charges can exist. Such electrical boundary conditions naturally lead to the existence of a maximum depolarizing field (denoted by $\langle \mathbf{E}_{\rm dep} \rangle$ and determined from the atomistic approach of [11]) inside the zero-dimensional ferroelectric for a non-vanishing polarization.

The second term of equation (1) mimics a screening of $\langle \mathbf{E}_{\rm dep} \rangle$ via the β parameter. More precisely, the residual depolarizing field resulting from the combination of the first and second terms of equation (1) has a magnitude equal to $(1-\beta)|\langle \mathbf{E}_{\rm dep} \rangle|$. $\beta = 0$ thus corresponds to ideal OC conditions, while an increase in β lowers the magnitude of the resulting depolarizing field. $\beta = 1$ corresponds to ideal short-circuit (SC) conditions for which the depolarizing field has vanished (that is, for which *all* the polarization-induced surface charges are screened).

The third and fourth terms of equation (1) represent the effect of an electric field, $\mathbf{E}$, and applied stress, σ, on properties of the investigated system, respectively [24]—with a being the five-atom lattice constant at 0 K and the sum over j in the fourth term running from 1 to 6 (as consistent with Voigt notations).

This effective Hamiltonian was used within both Monte Carlo (MC) and molecular dynamics (MD) simulations. In the MC scheme, the equilibrium dipolar and strain patterns were found by using a large number of MC sweeps (typically of the order of 40 000) to first equilibrate the system and then compute statistical averages—at each temperature, electric field and/or stress value. In order to find the dipolar pattern of the ground state, the temperature was decreased in small steps starting from high temperatures (for which the long-range dipolar order is absent). Within the MD technique, an alternating (ac) electric field was usually applied, and statistical quantities were computed as a function of time. As a result, hysteresis loops of the order parameters versus the field's value were obtained. Note that these MD simulations correctly reproduce the transition temperatures obtained within the MC approach, and also provide a good agreement with experiments for the soft mode frequency in bulk PZT [25].

3. Dipole vortices in zero-dimensional ferroelectrics

As discovered in [7, 8], stress-free ferroelectric nanodots under open-circuit conditions exhibit a ground-state structure consisting of a vortex for their local dipoles. Such a striking ground state is shown in figure 1 for the 12 × 12 × 12 BT (a) and PZT60 (b) dots, i.e. for two cubic nanodots of lateral size around 48 Å, as predicted by the effective Hamiltonian method described in section 2. Figure 1 indicates that no spontaneous polarization exists for the ferroelectric dots exhibiting the vortex pattern. This contrasts with magnetic dots for which a dipole vortex also exists but with a core possessing a magnetization [26]. The reason behind such a difference most likely lies in a stronger short-range interaction and weaker cubic anisotropy in magnets in comparison with ferroelectrics.

We decided to compare in figure 1 the dipole patterns obtained in 12 × 12 × 12 BT and PZT60 dots, mainly to

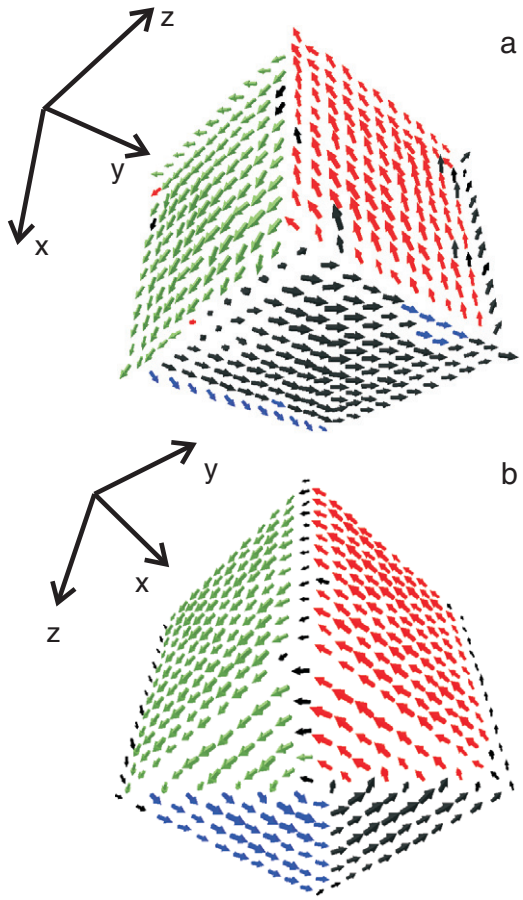

Figure 1. Dipole pattern, at 10 K, in 12 × 12 × 12 stress-free $BaTiO_3$ (a) and PZT60 (b) dots under OC electrical boundary conditions. The arrows show the direction of the dipole moments in the primitive unit cells. The *x*-, *y*- and *z*-axes are also indicated.

know if the fact that PZT60 and BT *bulks* have different ground states with dipoles lying along different directions affects the vortex structure in the corresponding nanodots (BT bulk has a rhombohedral ground state with dipoles pointing along a ⟨111⟩ direction [18] while the ⟨001⟩ directions are the possible directions for the polarization in the tetragonal ground state of *bulk* PZT60 [27]). Interestingly, and as indicated in [15], figure 1 reveals that the direction about which the vortex in the dots rotates is a possible direction of the polarization in the bulk. In other words, the direction of the vortex in the PZT60 nanodots is along a ⟨001⟩ direction while it is along a ⟨111⟩ direction in the BT dot. Figure 1(b) further tells us that one can also think of the vortex structure of the PZT60 ferroelectric dots as being made of four different domains, each having dipoles aligned a specific ⟨001⟩ direction, with 90° domain walls between the domains—which is a solution that was actually proposed many years ago by Kittel [28].

The *shape* of the nanodots also influences the dipole vortices, as has been shown in [8, 15, 29]. In particular, elongated dots can have several vortices with alternating chirality [8, 15]. Another source that affects the dipole vortex structure is the *size* of the nanodot, as emphasized by comparing figure 1(a) with figure 2—that displays the dipole pattern obtained in a 24 × 24 × 24 BT nanodot at 10 K [7]. In

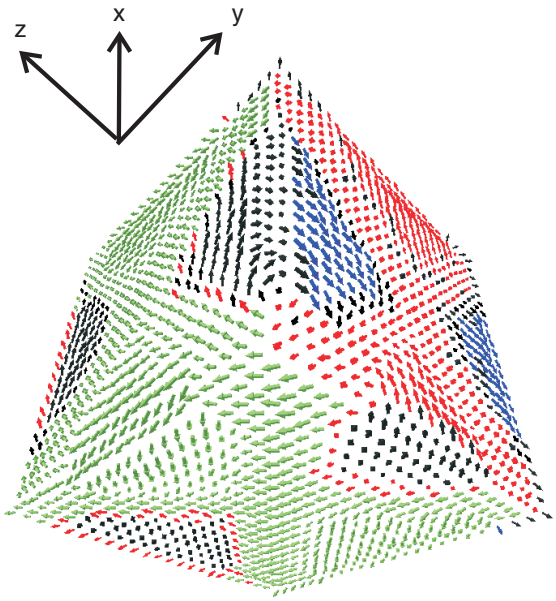

Figure 2. Dipole pattern, at 10 K, in a stress-free 24 × 24 × 24 $BaTiO_3$ dot under OC electrical boundary conditions.

this latter structure, the dipoles in the core of the dot organize a vortex about a ⟨111⟩ direction while additional vortices (that are absent in the small dot, see figure 1(a)) rotating about a ⟨001⟩ direction also form around *each* middle of the 12 cubic edges. Such a peculiar pattern yields the two cross-sections depicted in figure 3, that are a cross-section about the (111) plane passing through the dot's center (figure 3(a)) and a cross-section about the (001) plane corresponding to the 13th (001) atomic plane from the top of the dot (figure 3(b)).

Furthermore, it was previously shown [11] that the dipole vortices can occur even if a rather large amount of the maximum depolarizing field is screened by, e.g., external short-circuited metallic plates. Figure 4 shows the total energy of a PZT60 12 × 12 × 12 cubic nanodot as a function of the β parameter defined in section 2, and obtained at 1 K. As discovered in [11], two kinds of dipole pattern exist: for large β the dot is polarized, while β smaller than $\simeq$0.9 gives rise to the vortex structure. These two patterns are schematized in the insets of figure 4. Interestingly, decreasing β from its ideal-short-circuit value of unity first results in decreasing the total energy of the polarized dot in response to the increasing-in-magnitude depolarizing field (with the dipoles decreasing in magnitude when β decreases). Then, as soon as the vortex structure is created, the *average* electric field inside the vortex pattern is null, and thus no depolarizing field exists. As a result, the total energy (as well as the magnitude of the dipoles) does not depend on β anymore. One can also view figure 4 as displaying two straight lines (that intersect for $\beta \simeq 0.9$) that describe the dependence of the total energy on β for two different states, respectively, that is for the polarized state versus the vortex state. The fact that these two lines have very different slopes and intersect indicates that the β-driven phase transition from the polarized to the vortex state is of first order.

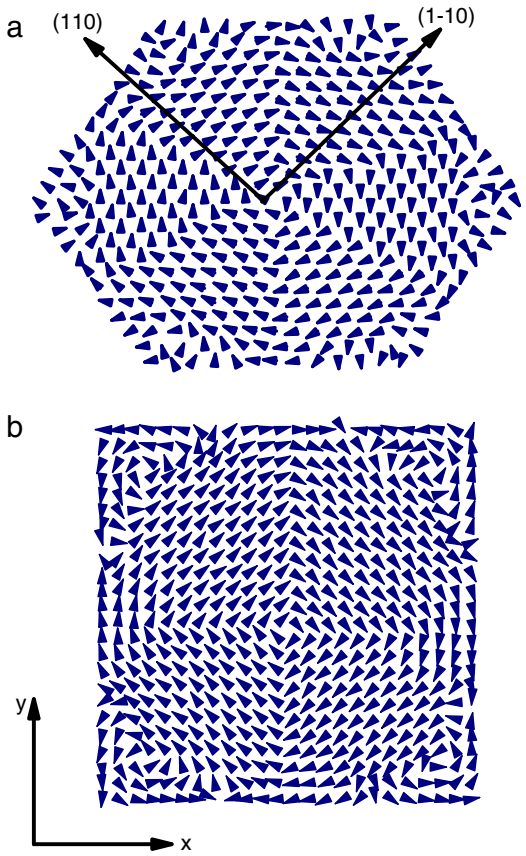

Figure 3. The cross-section of the dipole pattern, at 10 K, in a stress-free 24 × 24 × 24 $BaTiO_3$ dot under OC electrical boundary conditions in a specific (a) (111) plane and (b) (001) plane.

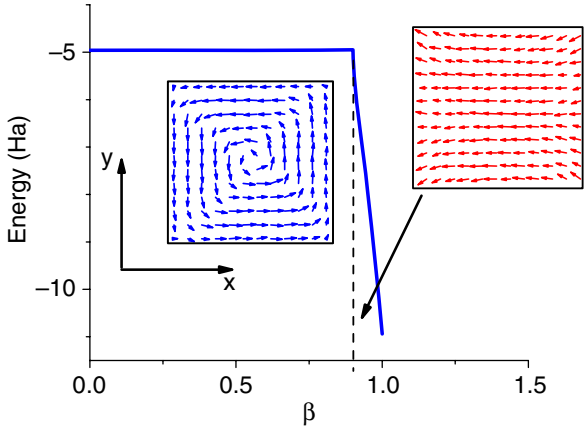

Figure 4. The dependence of the total energy, at 1 K, in a stress-free 12 × 12 × 12 dot of PZT60 (under OC electrical boundary conditions) on β. The insets show the corresponding stable dipole patterns.

4. Toroidal moment associated with dipole vortices in zero-dimensional ferroelectrics

As indicated in section 2, outputs of the effective Hamiltonian simulations include the local dipole moments, $\{\mathbf{p}_i\}$. Such outputs allow the computation of the following quantities:

$$\langle \mathbf{P} \rangle = \frac{1}{Nv} \sum_i \mathbf{p}_i$$
$$\mathbf{g} = \frac{1}{2Nv} \sum_i \mathbf{r}_i \times \delta \mathbf{p}_i \qquad (2)$$
$$\mathbf{G} = v\mathbf{g}$$

where v is the volume of the five-atom primitive unit cell, and $\mathbf{r}_i$ locates the center of unit cell i. $\langle \mathbf{P} \rangle$ is the polarization. $\delta \mathbf{p}_i$ is the difference between the dipole at cell i and the averaged (over all the cells) dipole, that is $\delta \mathbf{p}_i = \mathbf{p}_i - v\langle \mathbf{P} \rangle$. The quantity $\mathbf{G}$ is the so-called toroidal moment, which has been recently defined and investigated from phenomenology [30, 31] and first-principles-based computations [8, 11]. $\mathbf{g}$ provides the toroidal moment per unit volume. $\mathbf{G}$ or $\mathbf{g}$ can be considered as the right order parameter to characterize the formation and evolution of dipole vortices in ferroelectric dots, unlike the polarization (that vanishes for electric dipole vortices) [8, 11]. Interestingly, $\mathbf{g}$ (and thus also $\mathbf{G}$) is an axial vector in ferroelectric dots, and thus neither changes under the inversion of space nor is altered under time inversion symmetry [30]. On the other hand, because of the difference in symmetry between electric dipoles versus magnetic dipoles, the toroidal moment of magnetic dots is a polar vector and thus breaks both the space and time inversion symmetry [32].

For the vortices shown in figure 1(b), the direction of $\mathbf{g}$ in the PZT60 dot coincides with one of the ⟨001⟩ axes. Due to the cubic shape of this dot, the toroidal moment can also be parallel or antiparallel to any other ⟨001⟩ direction with equal probability. In other words, the ground state is sixfold degenerate. For the BT dot shown in figure 1(a), the toroidal moment can be along any ⟨111⟩ direction, implying that the ground-state vortex structure is eightfold degenerate.

Figure 5(a) presents the temperature dependence of the toroidal moment, as obtained by the effective Hamiltonian method for a 12 × 12 × 12 PZT60 nanodot under OC electric boundary conditions. One can see that the toroidal moment is null at high temperatures, while there is a temperature T_m (around 600 K, here) below which the z-component of the toroidal moment grows when further reducing the temperature (note that the polarization is numerically found to vanish for any temperature in this system). T_m is thus the highest temperature at which the dipoles adopt a vortex structure. On average, the local dipoles increase in magnitude upon cooling below T_m, which explains why the z component of $\mathbf{g}$ grows larger when decreasing the temperature below T_m.

Let us now briefly focus on ferroelectric rings rather than cubic dots. In this case, the toroidal moment is found to only very slightly increase when one first increases the internal diameter from its minimal value; see figure 6 (this behavior can be explained by the fact that the center of the dot does not contribute much to the toroidal moment, according to the simulations). It is only when the internal diameter becomes rather close to the outer diameter that the toroidal moment starts rapidly decreasing when further increasing the internal diameter, as indicated by figure 6.

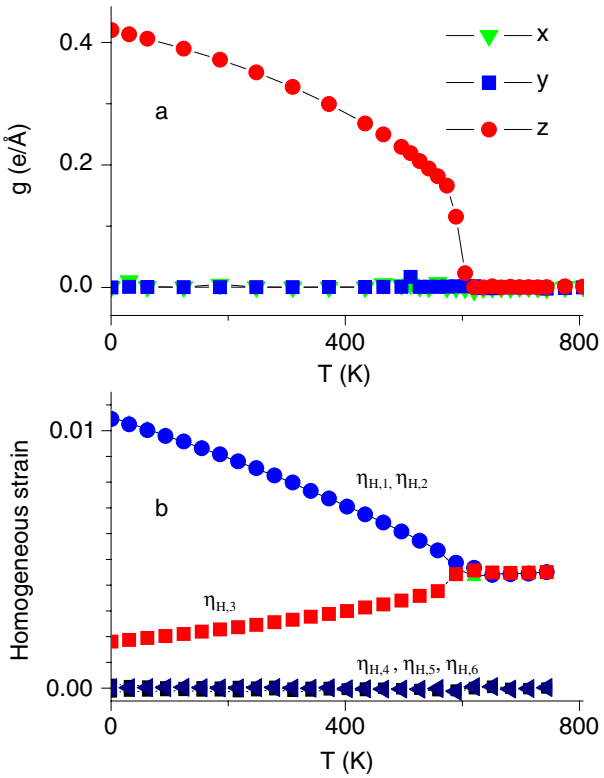

Figure 5. Temperature dependence of the toroidal moment (a) and homogeneous strain (b) in a stress-free 12 × 12 × 12 nanodot of PZT60 under OC electrical boundary conditions. The temperature has been rescaled to match the experimental Curie temperature of bulk PZT.

5. Strain characteristics of dipole vortices in zero-dimensional ferroelectrics

Figure 5(b) shows the temperature dependence of the *homogeneous* strain, $\{\eta_H\}$ (expressed in Voigt notation), in the 12 × 12 × 12 PZT60 nanodot under OC electric boundary conditions. One can see that, below T_m, the strain undergoes changes that are consistent with the appearance of the z-component of the toroidal moment. The component of the strain tensor associated with the direction of the vortex (i.e., $\eta_{H,3}$) is rather small, while $\eta_{H,1} = \eta_{H,2}$ exhibit much larger changes with temperature below T_m. One can also see that $\eta_{H,3}$ is smaller than $\eta_{H,2} = \eta_{H,1}$, below the temperature at which the vortex pattern forms. In other words, the tetragonal axial ratio c/a is lower than unity for the vortex in dots, which contrasts with the axial ratio in tetragonal systems exhibiting either a spontaneous polarization [27] or the condensation of antiferrodistortive motions [33]. Such a unique strain feature can be used to experimentally identify the vortex structure in ferroelectrics. (Note that another unique feature associated with a dipole vortex is its associated original electric field pattern close to the dot, as revealed by [15].)

Interestingly, [15] also reported that the *inhomogeneous* strain, $\{\eta_I\}$, exhibits striking features when a dipole vortex is formed in a ferroelectric dot. For instance, it was numerically found [15] that (1) $\eta_{I,1}$ is large in the regions of the dot having dipoles oriented along x and $-x$, while it is much smaller in the domains having the local modes in the y and $-y$ directions—because of the coupling between the dipoles making the vortex and the strain [18]; and (2) $\eta_{I,1}$ and $\eta_{I,2}$ are maximal in the center of the dot (as a result, cutting the core of the dot to make it a ring decreases the maximal value of $\eta_{I,1}$ and $\eta_{I,2}$, which can prevent the occurrence of cracks inside the dot, and thus stabilize the vortex dipole structure).

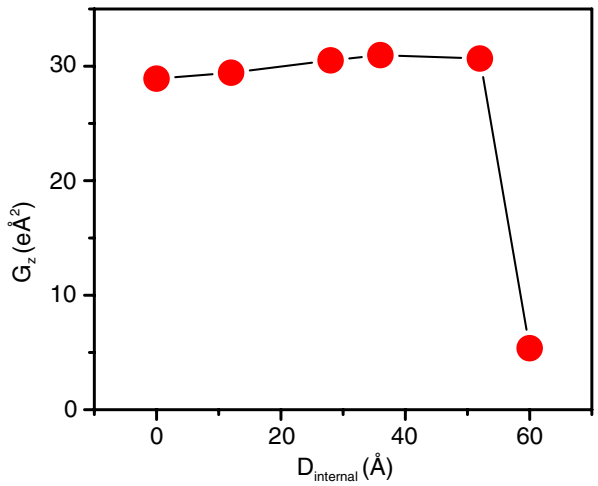

Figure 6. The dependence of the toroidal moment on the $D_{internal}$ internal diameter in nanotubes with height 56 Å and diameter 76 Å.

6. Novel electromechanical coupling in zero-dimensional ferroelectrics

In this section, a novel form of electromechanical coupling in ferroelectric dots, arising from the coupling between the toroidal toroidal moment and stress, is described [14]. To better appreciate it, let us first recall basic facts about piezoelectricity in a polar system. For this, it is useful to expand the thermodynamic potential, Φ, in linear order of external fields and stresses as a sum of four terms, following [34]. Such a decomposition is shown in the left column of table 1. The first and second terms correspond to the coupling between the polarization, **P**, and applied electric field, **E**, and to the coupling between the applied stress, σ, and the homogeneous strain, η_H, respectively. The third energy involves the d piezoelectric tensor, while the last term, Φ_0, gathers all the energies that are explicitly independent of both **E** and σ. As indicated in table 1, minimizing the derivative of the thermodynamic potential with respect to the applied field yields the mathematical equality associated with the so-called *direct* piezoelectric effect [34] (that characterizes the polarization's response to a stress). Similarly, the derivation of Φ with respect to σ leads to the *converse* piezoelectric effect—that represents the change of the shape of a material when subject to an applied electric field [34].

Now, we turn to a dipole vortex. For the toroidic systems, it is important to determine the thermodynamic potential containing a toroidal moment rather than a polarization. In particular, one may wonder how **g** enters such a potential, or, equivalently, to which quantity **g** is linearly coupled to provide

Table 1. Analogy between the **d** piezoelectric tensor in polar systems and the $\mathbf{d}^g$ axial piezotoroidic tensor in materials exhibiting an electric dipole vortex. Φ, **P**, **E**, σ, η_H, **g** and curl **E** represent the thermodynamic potential, polarization, electric field, stress, homogeneous strain, toroidal moment and the cross-product $\nabla \times \mathbf{E}$, respectively. The tensor components are indicated in Voigt or matrix notation. The 'eq' subscript is used to indicate the value of the properties at equilibrium, that is before applying a field or a stress. Einstein conventions are used for indicating the summations over j and i in the second and third rows.

Polarization	Electric dipole vortex
$\Phi = -(\mathbf{P} - \mathbf{P}^{eq})\mathbf{E} - (\boldsymbol{\eta}_H - \boldsymbol{\eta}_H^{eq})\boldsymbol{\sigma} + \mathbf{E}\mathbf{d}\boldsymbol{\sigma} + \Phi_0$	$\Phi = -(\mathbf{g} - \mathbf{g}^{eq})(\text{curl}\,\mathbf{E}) - (\boldsymbol{\eta}_H - \boldsymbol{\eta}_H^{eq})\boldsymbol{\sigma} + (\text{curl}\,\mathbf{E})\mathbf{d}^g\boldsymbol{\sigma} + \Phi_0$
$d\Phi/d\mathbf{E} = 0 \Rightarrow P_i = P_i^{eq} + d_{ij}\sigma_j$	$d\Phi/d\text{curl}\,\mathbf{E} = 0 \Rightarrow g_i = g_i^{eq} + d_{ij}^g\sigma_j$
$d\Phi/d\boldsymbol{\sigma} = 0 \Rightarrow \eta_{H,j} = \eta_{H,j}^{eq} + d_{ij}E_i$	$d\Phi/d\boldsymbol{\sigma} = 0 \Rightarrow \eta_{H,j} = \eta_{H,j}^{eq} + d_{ij}^g(\text{curl}\,\mathbf{E})_i$

a relevant energetic term. The answer to this question can be found from [35], where the combination of all energetic terms linear in **g** provides a coupling of **g** curl **E** with curl **E**, denoting the cross-product $\nabla \times \mathbf{E}$. Analogy was used to derive the third term of the thermodynamic potential for the materials exhibiting an electric dipole vortex [14]. More precisely, a new tensor, to be denoted by $\mathbf{d}^g$ and connecting curl **E** and σ, should exist in these materials, by analogy with the piezoelectric tensor **d** connecting **E** and σ in polar systems. As displayed in table 1, vanishing derivatives of Φ reveal that $\mathbf{d}^g$ should both characterize the response of the toroidal moment to an applied stress ('direct' effect) and the change of shape when applying an electric field with no vanishing curl—or, equivalently, a time-dependent magnetic field—('converse' effect). In other words, $\mathbf{d}^g$ represents a new kind of electromechanical coupling that should occur in ferroelectric nanodots—which may thus lead to the design of, e.g., transducers efficiently working at the nanoscale. This tensor differs in nature from the so-called polar piezotoroidic tensor introduced earlier for magnetic vortices and that connects the electric current density and strain [36, 37]. $\mathbf{d}^g$ also differs in symmetry from this polar piezotoroidic tensor, because (as already mentioned in section 4) the symmetry differences between magnetic and electrical dipoles imply that the toroidal moment in magnetic systems is a polar vector [32] while such a moment is an axial vector for the electric dipole vortices [30]. Based on these distinctions, $\mathbf{d}^g$ was named the '*axial* piezotoroidic' tensor [14]. Technically, $\mathbf{d}^g$ is an axial third-rank tensor—like the mathematical tensor associated with the so-called electrogyration effect [38]. As a result, and for instance, this tensor, in matrix notation, has four independent components for systems adopting a 4, $4/m$ or $\bar{4}$ point group [38]: $d_{31}^g = d_{32}^g$, d_{33}^g, $d_{15}^g = d_{24}^g$ and $d_{14}^g = -d_{25}^g$.

The existence of this new tensor was confirmed, as well as the sign and magnitude of its components being determined, in [14] by performing effective Hamiltonian Monte Carlo simulations on nanoparticles made of PZT60—which is the material of choice for 'traditional' piezoelectric applications. One convenient way to do this is to take advantage of the fluctuation–dissipation theorem [24, 39, 40] and of the outputs of the first-principles-derived approach (namely, the toroidal moment and strain at different Monte Carlo sweeps). Indeed, one can relate the axial toroidal moment to statistical averaging in the Gibbs framework: $\mathbf{g} = \langle \mathbf{g} \rangle = \sum_\mu \mathbf{g}^\mu \exp(-U^\mu/k_B T)/\sum_\mu \exp(-U^\mu/k_B T)$, where the index μ runs over the different possible states, k_B is the Boltzmann constant and $U = U_0 - V\mathbf{g}\,\text{curl}\,\mathbf{E} - V\boldsymbol{\sigma}\eta_H$, with U_0 gathering the terms of the internal energy that are independent of curl **E** and $\boldsymbol{\sigma}$. As analogous to the development of [39], it is straightforward to prove that taking the derivative of **g** with respect to σ leads to

$$d_{\alpha\beta}^g = \frac{V}{k_B T}[\langle g_\alpha \eta_{H,\beta}\rangle - \langle g_\alpha\rangle\langle \eta_{H,\beta}\rangle] \qquad (3)$$

where '$\langle\ \rangle$' denotes the average over the Monte Carlo sweeps. Equation (3) provides an efficient computation of the axial piezotoroidic tensor (that is, without applying any stress or electric field).

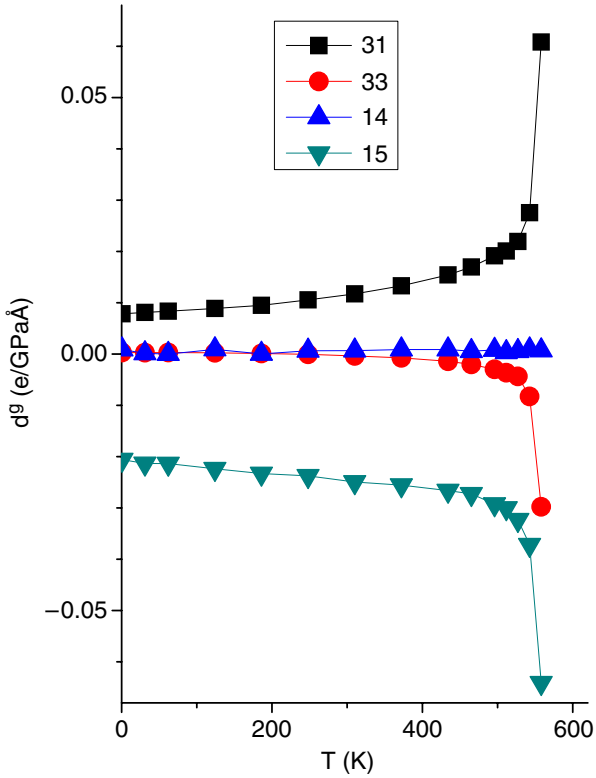

Figure 7. Temperature dependence of the piezotoroidic coefficients in a $12 \times 12 \times 12$ stress-free nanodot of PZT60 under OC electrical boundary conditions. The temperature has been rescaled to match the experimental Curie temperature of bulk PZT.

Figure 7 displays the temperature dependence of the independent elements of the axial piezotoroidic tensor for a cubic $12 \times 12 \times 12$ PZT60 nanodot under OC electric boundary conditions, as predicted by the use of the first-principles-based approach and equation (3). As shown in figure 5, decreasing the temperature below $T_m = 600$ K generates a toroidal

moment aligned along the z-axis (chosen to be parallel to the pseudo-cubic [001] direction). The PZT nanodot thus acquires a tetragonal symmetry with the $4/m$ point group, below T_m. Figure 7 reveals that the axial piezotoroidic effect indeed exists, below T_m, with the different non-zero coefficients (being those determined by symmetry arguments above) increasing (and nearly diverging) as the temperature is increased towards T_m—similar to piezoelectricity below the Curie temperature in 'normal' ferroelectrics [41]. In particular, one can see that the largest components are $d^g_{31} = d^g_{32}$ and $d^g_{15} = d^g_{24}$. This implies that devices made of PZT nanodots and aimed at efficiently converting mechanical input to electrical output should either use a stress applied along the x- and/or y-direction and takes advantage of the significant change of the toroidal moment along the z-direction, or apply a stress in the x oz plane (respectively, y oz plane) and detect the formation of the toroidal moment along the x (respectively, y) direction—especially close to T_m. Note that the d^g_{33} component is rather small, which indicates that a reasonable stress applied along the z-axis is not going to significantly modify the toroidal moment. Finally, d^g_{14} is found to vanish owing to an original symmetry element—namely, that combining the mirror element in the zx plane (and passing through the dot's center) with the simultaneous inversion of all the dipole moments leaves the vortex structure unchanged.

Additional effective Hamiltonian computations were also performed [14], in which a stress is directly applied to the nanoparticle. Small values of stress lead to axial piezotoroidic coefficients (calculated as the ratio between the change in the toroidal moment over the stress, see table 1) identical to those reported in figure 7. Moreover, a large enough stress can cause the toroidal moment to change in direction. For instance, applying a tensile uniaxial stress of 2 GPa along the initial (z) direction of the toroidal moment at 10 K results in the re-orientation of $\mathbf{g}$ from z to x or y axes, with equal probability. In other words, the stress is also capable of controlling the vortex's chirality, because of the new kind of electromechanical coupling that exists in ferroelectric nanodots.

7. Other novel tensors in zero-dimensional ferroelectrics

The axial piezotoroidic tensor is not the only new tensor that can appear in ferroelectric nanostructures. For instance, effective Hamiltonian simulations [14] revealed the existence of the tensor defined as $\boldsymbol{\chi}^g = \frac{1}{\varepsilon_0}\frac{\partial \mathbf{g}}{\partial \text{curl } \mathbf{E}} = -\frac{1}{\varepsilon_0}\frac{\partial \mathbf{g}}{\partial \dot{\mathbf{B}}}$, where ε_0 is the dielectric permittivity of vacuum and $\dot{\mathbf{B}}$ is the derivative of the magnetic field with respect to time [14]. By analogy with the 'normal' dielectric susceptibility tensor, such a new tensor was named as the electric toroidal susceptibility tensor [14]. It was computed as [14]

$$\chi^g_{\alpha\beta} = \frac{V}{\varepsilon_0 k_B T}[\langle g_\alpha g_\beta\rangle - \langle g_\alpha\rangle\langle g_\beta\rangle], \qquad (4)$$

following the use of the fluctuation–dissipation theorem [24, 39, 40]. Figure 8 shows the elements of the electric toroidal susceptibility tensor versus temperature, for a cubic 12 × 12 × 12 PZT60 nanodot under OC electric boundary conditions—as predicted by the use of the effective Hamiltonian approach and equation (4). These elements peak at T_m, that is at the temperature for which the nanoparticle acquires a toroidal moment (see figure 5(a)). Above this temperature, the three diagonal elements of this tensor coincide with each other, as consistent with the cubic symmetry. On the other hand, because of the tetragonal symmetry of the ground state, $\chi^g_{xx} = \chi^g_{yy} > \chi^g_{zz}$, below T_m.

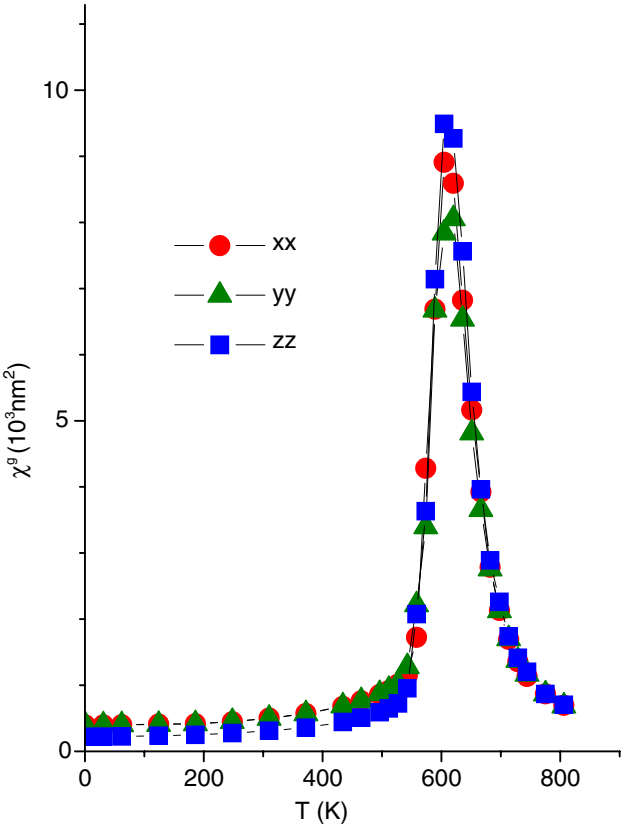

Figure 8. Temperature dependence of the toroidic susceptibility in a 12 × 12 × 12 stress-free nanodot of PZT60 under OC electrical boundary conditions. The temperature has been rescaled to match the experimental Curie temperature of bulk PZT.

Figure 5(a) also tells us that the value of the toroidal moment is sensitive to temperature below T_m. This automatically implies that there is a tensor, p^g, connecting the Cartesian components of the toroidal moment with a change in temperature. By analogy with the pyroelectric tensor (that links polarization with a change in temperature in polar systems), p^g can be named the pyrotoroidic tensor. Interestingly, the existence of p^g may open a new way to design nanosensors of infrared radiation. The existence of the pyrotoroidic tensor also implies that applying different curl of electric field (in a continuous way) in a system exhibiting electric dipole vortices should produce a change in temperature (that is, generate a new electrocaloric effect!) given by $\Delta T = -\frac{T}{C_{\text{curl }\mathbf{E}}}\int p^g_i \,\mathrm{d}(\text{curl }\mathbf{E})_i$, where $C_{\text{curl }\mathbf{E}}$ is the heat capacity at a constant curl $\mathbf{E}$—in the same manner that applying different electric fields in a polar system induces a change in temperature given by $\Delta T = -\frac{T}{C_E}\int p_i \,\mathrm{d}E_i$ (see [34]), where C_E is the heat capacity at a fixed electric field.

8. Phase transformation path from a vortex to a ferroelectric state in zero-dimensional ferroelectrics

Let us now discuss the phase transformation path, induced by homogeneous electric fields perpendicular to the vortex plane, in nanoparticles made of the technologically important PZT50 solid solution [12]. For this, effective Hamiltonian calculations were performed for PZT50 nanostructures of cylindrical shape (including nanodisks and nanorods), with diameter d ranging from 9 to 25 and height $h = 14$ (both are measured in units of bulk pseudo-cubic lattice parameter $a = 4.0$ Å). The crystallographic [001] direction was chosen as the cylindrical z-axis, with the [100] and [010] directions as the x and y axes, respectively. The initial dipole configuration of the vortex state was obtained from annealing simulations with temperature decreasing in small steps. A homogeneous electric field of varied strength was applied along the $+z$ direction at a fixed temperature of 64 K.

Figure 9 depicts the collective behaviors of the toroidal moment and net polarization that develop in a $d = 19$ nanodisk as the strength of electric field varies. When the electric field is small and below a critical value $E_{c,1} = 1.5$ V nm^{-1}, the disk shows only a non-zero z-component of the toroidal moment, G_z, while G_x and G_y are null. The system in this field region ($E \leqslant E_{c,1}$) thus retains the macroscopic toroid symmetry as in zero field (this structure phase will be denoted as phase I hereafter). As the field reaches $E_{c,1}$, G_z decreases only slightly as compared to the initial zero-field value, and meanwhile a large net polarization of 0.3 C m^{-2} develops. In fact, this magnitude of polarization is that of bulk BT. The vortex response of phase I is thus characterized by the coexistence of strong toroid moment and large polarization, both pointing along the cylindrical z-axis. It was further numerically found that the toroid moment in phase I responds to the **E** field by accurately following a quadratic scaling law of $G_z(E) = G_0 - bE^2$, where G_0 is the zero-field G_z moment and b is determined to be 285.5 e Å^4 V^{-2} for the $d = 19$ disk. (Note that this quadratic law leads to an interesting suggestion, that is, when a ferroelectric nanodisk is exposed to an alternating field $\mathbf{E}(t) = \mathbf{E}_0 \cos \omega t$, the toroid moment $\mathbf{G}(t)$ will respond with a double frequency 2ω, and thus its radiation field can be separated from that of vibrating polarization, which responds only with ω. The signal with 2ω frequency may further indicate whether it is associated with moment parallel or antiparallel to the z-axis, since the latter field is phase shifted by π with respect to the external applied field [31]. This suggestion may thus open an approach of using electromagnetic fields of pulse lasers to probe and/or read electric vortex state.)

The system behaves in a markedly different fashion when the electric field exceeds $E_{c,1}$, manifested in figure 9 by the occurrence of a non-zero G_y component and simultaneously a sharp decline of the G_z component. Being perpendicular to the initial G_z moment, the appearance of the G_y moment deviates the system from a macroscopic cylindrical symmetry. The nanodisk therefore undergoes a phase transformation to a new structure of different symmetry (this new structure will be denoted as phase II). Assuming that the dipoles

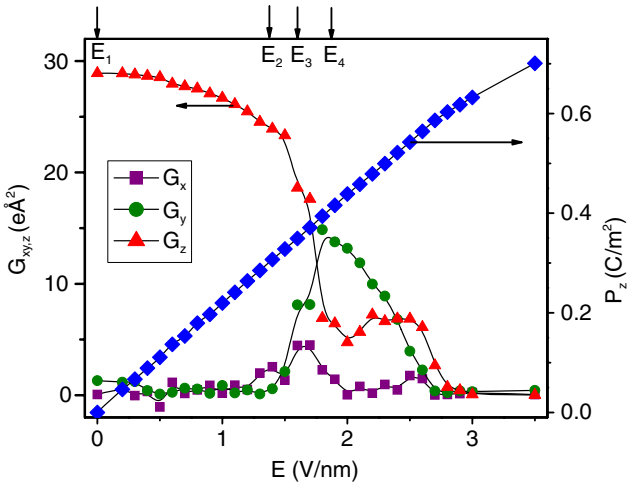

Figure 9. Toroidal moment **G** (using the left vertical axis) and net polarization P_z (using the right vertical axis) versus electric field in a $d = 19$ stress-free PZT50 disk under OC electrical boundary conditions. Arrows on the top horizontal axis indicate the selected electric fields for which the dipole configurations are analyzed in figure 10.

respond by collectively rotating toward the field direction, one would anticipate that the drastic decrease of G_z would be accompanied by a sharp rise in the polarization. Surprisingly, the net P_z polarization in figure 9 apparently does not feel the drastic variation of the toroid moment, and remains, to the naked eye, fairly smooth. As the electric field exceeds a second critical value $E_{c,2} = 2.8$ V nm^{-1}, all **G** components vanish and the system becomes a phase of pure polarization. The low-symmetry phase II thus acts as a key intermediate state bridging the transformation from phase I (of the same cylindrical symmetry as the initial vortex) to the destination phase of uniform polarization (that also has cylindrical symmetry).

Furthermore, figure 10 shows the dipole patterns for four different fields, denoted as E_1, E_2, E_3 and E_4, respectively (these fields are also indicated via arrows in figure 9). Looking at the dipole patterns at E_1 and E_2 fields shows that the vortex response in phase I is characterized by the collective rotation of dipoles towards the field direction. Particularly, it was found that this rotation process begins with (namely, is initiated by) dipoles near the cylindrical axis, which is consistent with the fact that a large strain exists in the vortex center [15] and that the rotation reduces this strain energy. The rotation is found to maintain cylindrical symmetry in the sense that dipoles within the same distance from the central axis respond equivalently.

As the field slightly changes from E_2 to E_3, two striking phenomena occur: (1) the dipole vortex in the xy plane shifts from the center; (2) another *lateral* vortex—for which the corresponding toroidal moment points along the y-axis—starts to nucleate near the surface.

A further increase of electric field from E_3 to E_4 leads to increasing the volume occupied by the new vortex and simultaneously decreasing the volume occupied by the in-plane vortex. The system at the E_4 field is thus characterized by the formation of a vortex-free ferroelectric region on one side—and a vortex region with a toroidal moment about the y-axis

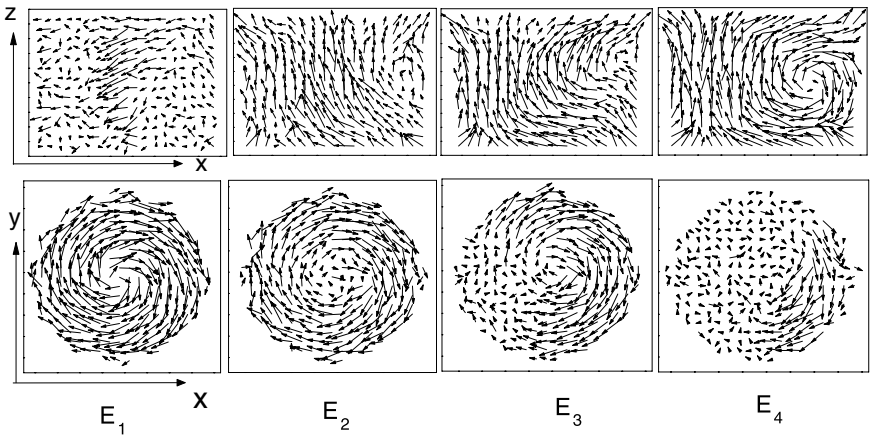

Figure 10. Configurations of local dipoles on the central xy cross-section (lower panel) and on the central xz cross-section (upper panel) in the $d = 19$ disk, at selected fields E_1, E_2, E_3 and E_4 as marked by the arrows in figure 9. The magnitude of each dipole is enlarged for clarity.

occurring on the other side. Interestingly, despite the fact that the formation of the lateral G_y vortex forces some dipoles to point opposite to the field direction between E_3 and E_4 fields, the net P_z polarization nonetheless still increases, as seen in figure 9. Finally, when the electric field continues to further increase above E_4, the ferroelectric region expands by extruding the center of the G_y lateral vortex toward the right-side surface, and this G_y vortex eventually disappears at the critical $E_{c,2}$ field.

The presence of phase II (with a toroid moment rotated by 90° with respect to the initial G_z vortex) raises an interesting question of what may happen when one starts with this phase (e.g., at $E = 2$ V nm^{-1}) and then decreases the electric field. The simulations reveal that, regardless of whether the field is gradually reduced or suddenly switched off, the system in phase II does not transform back to the initial state of G_z toroid moment, and instead is trapped in the G_y vortex state. More specifically, as the field is reduced, the G_y vortex at the E_4 field in figure 10 *grows* by moving its core toward the cylindrical axis (not toward the right-side surface), resulting in a pure vortex state with a G_y moment and $\mathbf{P} = 0$. This leads to a hysteresis, which is interesting in the sense that (i) the hysteresis is caused by the toroidal moment, not the polarization; (ii) it exists in a single particle of nanometer size; (iii) during the hysteresis, the toroidal moment is rotated rather than switched to the opposite direction. The G_y and G_z phases at zero field were further found to be very close in energy; the latter is lower by ∼1 meV per five-atom unit cell. Trapping of the system in the G_y state also suggests that this state is stable and surrounded by an energy barrier. To confirm this, the system of the G_y phase is heated at zero field to a chosen temperature $\tilde{T}$ and then cooled down to 64 K. It was found that only when $\tilde{T}$ is above 500 K is the G_y phase able to overcome the barrier and become the G_z phase.

Analysis showed that, in addition to the reduction of the depolarizing field, there is another factor that facilitates the transformation from phase I into phase II, that is, the interaction between local mode and strain. At zero field, the lattice of the vortex state is pseudo-tetragonal with a c/a ratio less than unity, i.e., $\eta_{H,1} = \eta_{H,2} > \eta_{H,3}$, because all dipoles are lying in the xy plane. As the field increases, the c/a ratio rises as a result of the polarization–strain coupling. Notably, the field at which c/a becomes unity (i.e. the system becomes pseudocubic) is very close to the critical $E_{c,1}$ field where phase I is transformed into phase II. The mode–strain coupling $-\sum_i |B|(\eta_{H,1}u_{ix}^2 + \eta_{H,2}u_{iy}^2 + \eta_{H,3}u_{iz}^2)$ advances the transition into phase II largely due to the increase in atomic volume, $\Delta v/v_0 = \eta_{H,1}+\eta_{H,2}+\eta_{H,3}$, which is nearly a constant in phase I and rises sharply for $E > E_{c,1}$.

9. Control of dipole vortices in zero-dimensional ferroelectrics

It is important to realize that toroidic phases are usually degenerated (e.g., the toroidal moment can be equivalently parallel or antiparallel to the z-axis, that is, the vortex can possess different chiralities). Let us imagine that a large number of ferroelectric particles are arranged into regular arrays, and that we know of a way of switching the chirality of the vortex of any dot in this array (note that any dipole vortex produces an electric field that has reasonably large values only very close to the dots [15]—which implies that the vortex structure in a single nanoparticle should thus be switchable without modifying the states of its neighboring particles, and thus that we avoid the so-called 'cross-talk' problem). Consequently, the toroidal carriers of information can thus be packed considerably more densely than the conventional carriers of polarization, giving rise to a dramatic improvement in the storage density of ferroelectric memories [8]. For instance, the minimum diameter that was found to be able to generate bistable toroid states is 3.2 nm [8]. This produces an ultrahigh storage density of 60 Tbits inch^{-2}, which is five orders of magnitude (!) larger compared to current nonvolatile ferroelectric random access memories' capability of 0.2 Gbits inch^{-2}. Such a promising capability also far surpasses the 1 Gbits inch^{-2} density of typical magnetic recording.

In other words, the existence of dipole vortices in zero-dimensional ferroelectrics holds tremendous promise for nanotechnology, but, to fulfill such promise, one has to solve

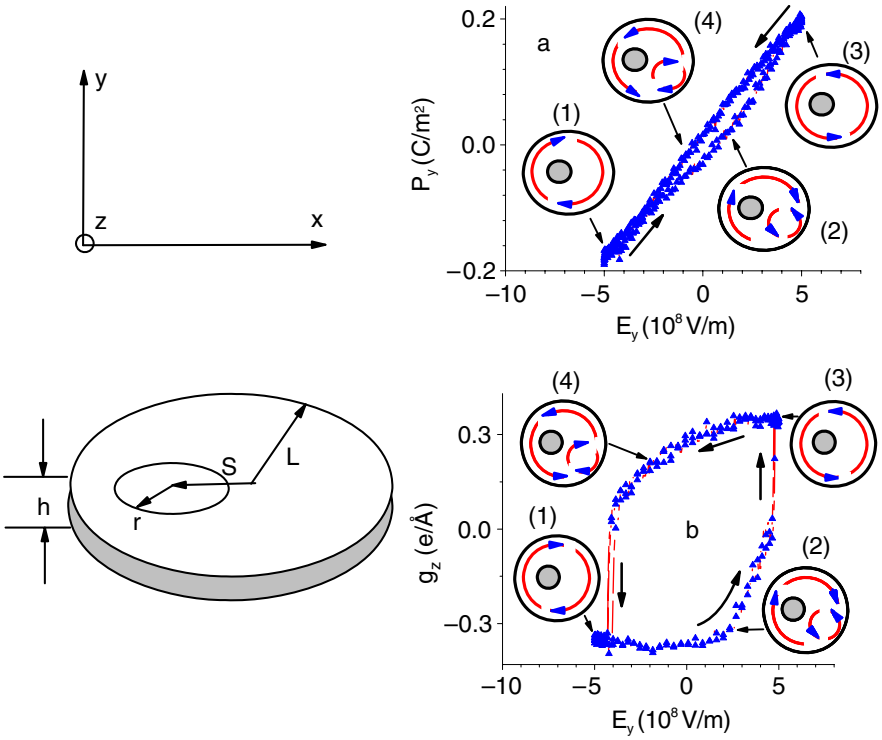

Figure 11. Predicted hysteresis loops in asymmetric stress-free PZT60 rings under OC electrical boundary conditions. Panels (a) and (b) show the evolution of the polarization and electric toroidal moment, respectively, versus the applied homogeneous ac electric field. Insets schematize the rings' geometry and the dipole arrangement in the (x, y) plane for the states (i)—where i ranges from 1 to 4; see the text.

the challenging problem of controlling the vortices' chirality. As a matter of fact, electric vortices can *not* directly couple with *homogeneous* electric fields [13, 15, 31, 37]. On the other hand, the electric toroidal moment can directly interact with curl **E**, according to classical electrodynamics [35]—implying that one way to control vortices is via the application of a curling electric field. A second possibility to control electric dipole vortices and their chirality is by applying (static) *inhomogeneous* electric fields, as revealed by the effective Hamiltonian simulations of [13].

Here, we would like to focus on a third possibility (that we found very promising, mostly because it should be easier to technologically implement it) for the control of electric vortices, that is by applying a *homogeneous* electric field to ferroelectric nanodots that are asymmetric in shape [17]. For this, an asymmetric nanoring made of PZT60, under stress-free and OC boundary conditions, was considered in [17]. The height, and internal and external radii about the z-axis (that lies along the [001] pseudo-cubic direction), of the investigated rings were denoted by h, r and L, respectively. Moreover, the center of the internal radius in any (001) plane was allowed to shift along the x-axis (that lies along the [100] pseudo-cubic direction) from the center of the external radius by a distance to be called S—as indicated in the inset of figure 11. The geometrical parameters in the effective Hamiltonian computations were taken to be $h = 24$ Å, $L = 32$ Å, $r = 8$ Å and $S = 12$ Å. Practically, the total energy of equation (1) was used in MD simulations to obtain the dipole configurations of the studied ferroelectric nanosystem under an *ac* homogeneous electric field of 10 GHz frequency[5] and applied along the y-axis.

Figure 11 displays the behavior of the y-component of the polarization (P_y) and of the z-component of the electric toroidal moment (G_z) of the investigated asymmetric ferroelectric nanoring as a function of the y-component of the electric field (E_y), respectively, at a simulated temperature of 300 K. Practically, E_y varies between -5×10^8 V m^{-1} and $+5 \times 10^8$ V m^{-1} depending on the simulated time. The insets of figure 11 display the schematization of four states of particular interest in the ferroelectric nanoring. State (1) is a vortex state characterized by a significantly *negative* G_z, that is polarized and occurs for the largest *negative* field values. State (2) differs from state (1) by having a much smaller polarization and, especially, by forming two vortices: one vortex that is reminiscent of state (1), and the second one that has nucleated inside the dot and that is not only of smaller dimension but also of opposite chirality to the first vortex. Such a striking state can be classified as an antiferrotoroidic pair state [16]. State (3) is also a vortex state like state (1), but of *opposite* sign for its G_z and P_y, and occurs for the largest *positive* investigated fields. State (4) resembles state (2) after reversing the chiralities of both the large and small vortices. Figure 11 thus indicates that it is possible

[5] Frequencies for the ac fields were chosen to be below the resonant frequencies to be in the quasi-adiabatic regime. Such resonant frequencies are numerically found to be in the order of THz for the studied ferroelectric nanorings.

to control the chirality of vortices by applying homogeneous fields in asymmetric ferroelectric nanorings, via the transition to intermediate (antiferrotoroidic) states, in the same manner that a homogeneous *magnetic* field is able to control the chirality of *magnetic* vortices in asymmetric *ferromagnetic* rings, via the transition into intermediate (onion) states [6]. Interestingly, states (2) and (4) were found to first deform themselves via the growth in size of their second vortex before transforming into the vortex states (3) and (1), respectively. Furthermore, no systematic controllable switching of the vortex chirality was found [17] when applying homogeneous electric fields in ferroelectric nanorings that are *symmetric* (that is for which $S = 0$)—which undoubtedly indicates that asymmetry is of crucial importance for the switching of the vortex chirality by a homogeneous field. This leads to the two following questions: (i) how can a *homogeneous* electric field control ferroelectric vortices, respectively, while this field is not allowed to directly couple with the electrical toroidal moments [31]—as symmetry arguments tell us (the electric field is a polar vector while the electric toroidal moment is an axial vector); and (ii) why does such control only occur in *asymmetric* systems?

To answer these questions, a vector, $\mathbf{R}$, characterizing the system's asymmetry was first defined in [17]. For instance, for the investigated asymmetric nanorings, the following vector representing the asymmetry-induced shift in center of gravity of the ring was introduced: $\mathbf{R} = \mathbf{x}r^2S/(L^2 - r^2)$, where $\mathbf{x}$ is the unit vector along the x-axis. The cross-product of this vector with the electric field, $\mathbf{R} \times \mathbf{E}$, has exactly the same symmetry as the electric $\mathbf{g}$ toroidal moment since both are axial vectors. One can thus consider, on sole symmetry grounds, an interaction energy in asymmetric ferroelectrics that is directly proportional to $(\mathbf{R} \times \mathbf{E}) \cdot \mathbf{g}$. Such an energy is non-zero in the considered cases because (i) the dot is asymmetric (i.e., S and thus $\mathbf{R}$ do not vanish), (ii) $\mathbf{R}$ is oriented along the x-axis, while $\mathbf{E}$ is along the y-axis and $\mathbf{g}$ lies along the z-axis. The existence of such a new energy was numerically confirmed by performing calculations in which $\mathbf{R}$ and $\mathbf{E}$ are purposely chosen to lie along the same axis (in this case, no possible control of the chirality of the electric vortices was found) or in which the magnitude of $\mathbf{R}$ is increased (in this case, we need a smaller electric field for switching the vortex chirality). Thus, $\mathbf{R} \times \mathbf{E}$ can be thought of as a field that can control the chirality and magnitude of the electric toroidal moment, $\mathbf{g}$, via an interaction energy proportional to $(\mathbf{R} \times \mathbf{E}) \cdot \mathbf{g}$ in asymmetric ferroelectrics.

Interestingly, this latter energy term also opens the way for attractive new technologies, e.g. to make *nanomotors* from asymmetric rings. As a matter of fact, purposely choosing a $\mathbf{R} \times \mathbf{E}$ vector that does *not* initially lie along the same direction as $\mathbf{g}$ will force the ring to rotate if this ring is free to do so—in the same manner that a macroscopic magnet can rotate when subject to a homogeneous magnetic field lying away from its magnetization [42]. (Note that for a continuously rotating nanomotor, the electric field must continue to rotate so that the ring must follow. This statement must be qualified by the fact that once the rotor is up to synchronous speed a field oscillating along one axis will suffice.)

10. Embedded ferroelectric dots

All the results discussed and displayed so far concern *isolated* zero-dimensional ferroelectrics. The aim of this section is to discuss properties of dots made from one kind of perovskite material, to be denoted by $AB''O_3$, that are rather *embedded* into a matrix made from *another* kind of perovskite material, to be denoted by $AB'O_3$. The total energy of equation (1) was extended by introducing a new energetic term that is related to the onsite contribution of alloying [16]. Such a term involves two different parameters for the $AB'O_3$ and $AB''O_3$ systems, that are denoted as $\kappa(AB'O_3)$ and $\kappa(AB''O_3)$, respectively, and that characterize the magnitude of the ferroelectric instability of these two systems [18]. Note that the existences of these two parameters are consistent with the direct first-principles results of [43]. The 'ferroelectric strength' of $AB'O_3$ and $AB''O_3$ simple systems was artificially adjusted by playing with the $\kappa(AB'O_3)$ and $\kappa(AB''O_3)$ parameters. For instance, a large negative (respectively, positive) $\kappa(AB''O_3)$ leads to a strong ferroelectric instability (respectively, no ferroelectric instability) of the pure $AB''O_3$ material. In the following, we will denote $\Delta\kappa$ as the difference between the two alloying-onsite parameters, i.e. $\Delta\kappa = \kappa(AB'O_3) - \kappa(AB''O_3)$. With the exceptions of the adjustable $\kappa(AB'O_3)$ and $\kappa(AB''O_3)$ variables, all the parameters of this toy model are those derived for the PZT50 solid solution from first-principles calculations [20]. (Such parameters yield a tetragonal ferroelectric ground state with a polarization pointing along a $\langle 001 \rangle$ direction and a Curie temperature $\simeq$ 1000 K, in the PZT50 bulk.) As a result, it was numerically found that $\kappa(AB''O_3)$ or $\kappa(AB''O_3) \simeq +0.0094$ au is the highest value to have a ferroelectric ground state in pure $AB'O_3$ or $AB''O_3$ material, respectively.

Figure 12 shows the temperature-versus-$\Delta\kappa$ phase diagram of a 16 × 16 × 16 periodic supercell (20 480 atoms, 64 Å lateral size) containing an $AB''O_3$ cubic dot of 48 Å lateral dimension embedded in a host matrix made of pure $AB'O_3$. Practically, for *positive* $\Delta\kappa$, $\kappa(AB''O_3)$ is set to zero while $\kappa(AB'O_3)$ is allowed to vary. These cases thus correspond to a specific ferroelectric dot immersed in different media that are all ferroelectrically harder than the dot and that can either be ferroelectric (small positive $\Delta\kappa$) or paraelectric (larger positive $\Delta\kappa$). The reverse situation applies for the case of *negative* $\Delta\kappa$: $\kappa(AB''O_3)$ is varied while $\kappa(AB'O_3)$ vanishes, implying that either ferroelectric dots with smaller ferroelectricity strength than the medium (for small negative $\Delta\kappa$) or paraelectric dots (for larger negative $\Delta\kappa$) inserted in a matrix made from a specific ferroelectric material were mimicked.

Figure 12 reveals the existence of six different phases, for which the associated dipole patterns are displayed in insets (phase boundaries were practically determined by identifying the peak or abrupt jumps of the susceptibilities altogether with the appearance of the spontaneous polarization or toroidal moment). Two of these phases are expected based on previous knowledge of ferroelectrics: the paraelectric, PE, state at high temperature, and the ferroelectric, FE1, phase occurring at intermediate and low temperature when $\Delta\kappa$ is small in

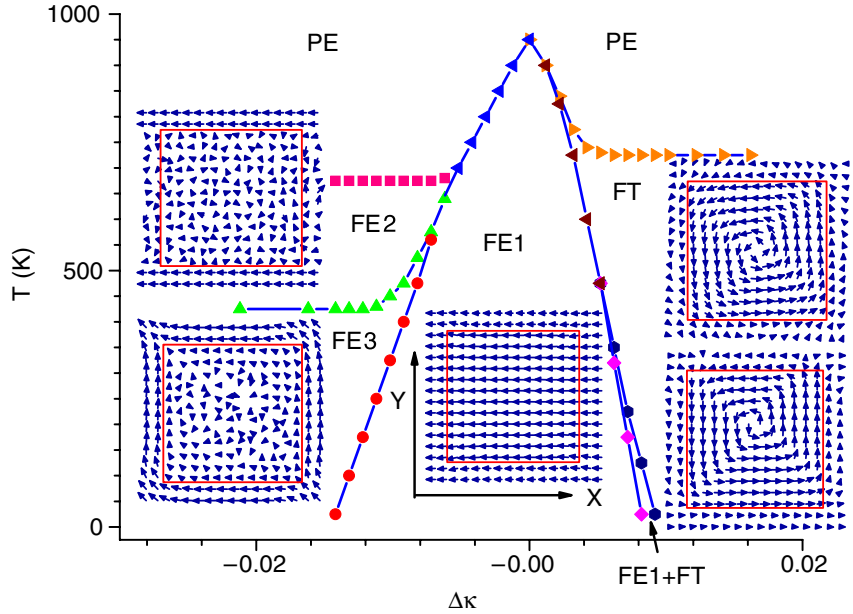

Figure 12. Temperature-versus-$\Delta\kappa$ phase diagram of a $12 \times 12 \times 12$ $AB''O_3$ dot embedded in a $AB'O_3$ medium within a $16 \times 16 \times 16$ periodic supercell. The positive $\Delta\kappa$ part of this diagram corresponds to a soft ferroelectric dot immersed in a medium that is ferroelectrically harder than the dot and that has a decreasing ferroelectric instability as $\Delta\kappa$ increases. The negative $\Delta\kappa$ part of this diagram corresponds to a dot (having a ferroelectric instability that is weaker than those of the medium and that decreases, and then vanishes, as $\Delta\kappa$ increases in magnitude) embedded in a ferroelectrically soft medium. The lines with symbols represent the phases' boundaries. The insets show a (001) cross-section of the dipole configuration in the different phases. Specifically, these insets correspond to atomistic calculations with the following ($\Delta\kappa$, temperature) combination: (−0.0212 au, 1 K), (−0.0212 au, 500 K), (0.0062 au, 1 K), (0.0087 au, 1 K) and (0.0112 a.u., 1 K) for the FE3, FE2, FE1, FE1 + FT and FT phases, respectively. The dot surfaces are indicated via thick continuous lines in these insets. The x- and y-axes are chosen along the pseudo-cubic [100] and [010] directions, respectively.

magnitude. In this FE1 state, both the dot and medium develop homogeneous parallel dipoles—with these dipoles being larger (smaller) in the dot than in the host when $\Delta\kappa$ is positive (negative), as consistent with the definition of $\Delta\kappa$ (i.e. the difference between the onsite parameters of the medium and the dot).

Four phases of figure 12 can be considered as novel structures. They are denoted as FT, FE1 + FT, FE2 and FE3, respectively. The FT phase, which occurs for the largest positive $\Delta\kappa$ values, exhibits a finite toroidal moment. The appearance of this state in this region of the phase diagram results from the fighting of the dipoles in the dot against the large enough depolarizing field [7, 8, 11] (which arises from the significant non-similarity between the 'more ferroelectric' dot and 'less ferroelectric' host material). The present discovery of this FT phase is, in fact, consistent with the previous finding that *isolated* ferroelectric dots surrounded by vacuum exhibit a vortex structure for their dipoles below a critical temperature [7, 8, 11], because one can think of vacuum as a medium having an infinite positive value for $\kappa(AB'O_3)$. However, and unlike in the vacuum, the dipoles of the host matrix in the FT phase become slightly polarized by the nearby dipoles located inside the dots and near the surfaces, when this host matrix is still rather 'soft' (see the corresponding inset of figure 12). For such cases, the medium thus also generates a toroidal moment that is parallel to, but of lower magnitude than, the one solely associated with the dot.

Moreover, the FE1 + FT phase appearing in the phase diagram at small temperature and within a narrow range of positive $\Delta\kappa$ is rather remarkable because it displays an unusual cohabitation between the toroidal moment and the spontaneous polarization. In this phase, the medium generates an electric field inside the dot, that (as in some magnetic nanodots under an external magnetic field [44]) leads to the shift of the vortex structure with respect to the center of the dot (see the corresponding inset in figure 12) and thus activates a polarization. Note, too, that this FE1 + FT phase can be considered as a low-temperature bridging structure between the FE1 and FT phases since it was numerically found that the FE1-to-FE1 + FT and FE1 + FT-to-FT transitions are second order in character, unlike the FT-to-FE1 phase transition that displays all the expected features of a first-order phase transition (e.g., the toroidal moment suddenly disappears at this boundary in favor of a *finite* value of the polarization, and the FT-to-FE1 boundary line has a rather large thermal hysteresis: it is typically increased by $\simeq$100 K with respect to the one displayed in figure 12 when heating, rather than cooling).

The last two phases, FE2 and FE3, appearing in figure 12 are both ferroelectric and occur at intermediate and low temperatures, respectively, for the largest negative values of $\Delta\kappa$. In other words, these two states correspond to cases for which the dot, unlike the medium, is made of a material that desires to be paraelectric. As a result, the FE2 phase exhibits a spontaneous polarization that originates from the alignment along a $\langle 001 \rangle$ direction of dipoles belonging to some *specific regions of the medium*. More specifically, these regions belong to the {001} planes that contain the polarization direction and

that do not possess any site belonging to the dot (see, e.g., the corresponding inset of figure 12 for FE2 showing the homogeneity of dipoles in the top and bottom planes, while the parts of the medium located at the right and left sides of the dot do *not* display any homogeneity for their dipoles). The reason behind such a unique arrangement, in which the largest dipoles in the medium intentionally avoid pointing towards the dots, is once again the minimization of the depolarizing energy. When decreasing the temperature, the FE2 phase transforms into the FE3 state, that is associated with a polarization that has now two non-vanishing components along two different ⟨001⟩ directions. More precisely, the corresponding inset of figure 12 reveals that, in the FE3 phase, the top and bottom parts of the medium exhibit dipoles that are similar in direction to those in the FE2 phase, while dipoles located in the medium at the right and left sides of the dot have dipoles aligned along a *perpendicular* direction. Such a dipole arrangement arises, once again, from a minimization of the depolarizing energy. Interestingly, the FE2 and FE3 phases bear resemblance to some states that were experimentally found recently in artificially constructed magnets [45]. Moreover, note that it was numerically found that another solution (but of slightly higher energy than that of the FE3 phase) is possible at low temperature for large negative $\Delta\kappa$: it consists of the top and bottom parts of the medium having dipoles homogeneously aligned a specific ⟨001⟩ directions (as in the FE2 phase) while the dipoles of the medium located on the right and left sides of the dot form a vortex structure.

It was also numerically checked that all the phases of figure 12 still occur when varying the size of the dot or the size of the whole supercell [16]. Moreover, of these six states, the FT and FE1 + FT phases are the sole structures that refine themselves when allowing *several* $AB''O_3$ dots to be present in a supercell possessing a $AB'O_3$ medium. For large enough positive $\Delta\kappa$, neighboring dots have vortices rotating in an *opposite* fashion [16]. In other words, the FT and the FE1 + FT phases of figure 12 should in fact become the AFT and FE1 + AFT states shown in figure 13, respectively, when dots are close enough to each other (as in the above dots' arrays). Such novel *antiferrotoroidic* phases, unlike the FT and FT+FE1 states, allow the dipoles located *between* two adjacent dots to all point along similar directions, which minimizes the corresponding domain wall energy at the cost of the electrostatic interaction between neighboring vortices (it was numerically found that the direct electrostatic interaction between two different toroidal moments should align these moments along the same direction—that is, it should lead to a ferrotoroidic, rather than antiferrotoroidic, order [15]). Furthermore, the centers of the vortices in the FE1 + AFT phase form a rather unusual lattice (see, e.g., that the centers of the vortices have different y-locations for dots that are adjacent along the x-axis). This unique geometry originates from the desire of the whole system to maximize the number of its dipoles (in the dots) lying along the polarization direction, considering the underlying antiferrotoroidic order.

Interestingly, the various dipole patterns of embedded dots, and their corresponding different susceptibilities, may lead to the design of materials possessing a negative index of refraction—which is of technological importance [46] because, e.g., it makes an object opaque to external radiations.

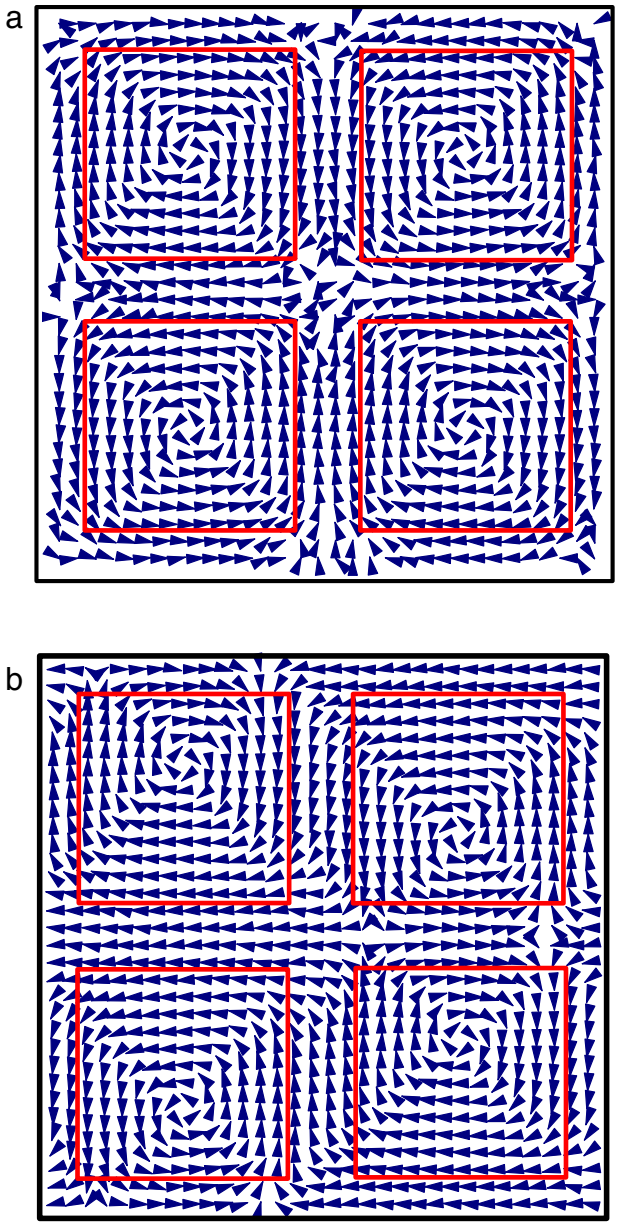

Figure 13. (001) cross-sections of the dipole configuration in the AFT and FE1 + AFT phases in panels (a) and (b), respectively, for four 12 × 12 × 12 $AB''O_3$ dots embedded in a $AB'O_3$ medium within a 32 × 32 × 32 periodic supercell. Such cross-sections specifically correspond to atomistic calculations for which the ($\Delta\kappa$, temperature) combination is (0.0112 au, 1 K) and (0.0087 au, 1 K) for the AFT and FE1 + AFT states, respectively. The dots' surfaces are represented by thick continuous lines. The x- and y-axes are chosen along the pseudo-cubic [100] and [010] directions, respectively.

11. Conclusions

In summary, we have reviewed some recent articles [7, 8, 11–17] devoted to the study of dipole vortices in zero-dimensional ferroelectrics, via the use of the effective Hamiltonian method described in section 2. In particular,

we discussed the dependency of the morphology of these vortices on the size and shape of the nanoparticle, on the material from which the nanoparticle is made, its electrical boundary conditions and its surroundings (that is, isolated nanoparticles versus particles embedded in a polar matrix). We also emphasized that dipole vortices exhibit unique strain characteristics (as well as briefly mentioning that they also produce an original electric pattern), which can be put to use to *experimentally* find these vortices' structures. The need to use the electric toroidal moment as the right order parameter to describe the formation and evolution of these vortices was also discussed at length. Moreover, the existence of various tensors of fundamental and technological interest (e.g. the piezotoroidic, electric toroidal susceptibility and pyrotoroidic tensors), and linking the toroidal moment to other physical quantities, was also established. We also described in detail an original path between the vortex and ferroelectric/polarized states, and discussed original ways of controlling the chirality of the dipole vortices. We thus hope that this review will be of high benefit to scientists and engineers working in the fascinating field of dipolar nanostructures.

Acknowledgments

This review is supported by DOE grant DE-FG02-05ER46188, ONR grant N00014-04-1-0413 and NSF grants DMR-0701558, DMR-0404335, DMR-0080054 (C-SPIN), MRI-0421099 and MRI-0722625. SP also appreciates grants RFBR-07-02-00099 and 05-02-90568NNS.

References

[1] Fernandez A and Cerjan C J 2000 *J. Appl. Phys.* **87** 1395
[2] Aharoni A 1990 *J. Appl. Phys.* **68** 2892
[3] Schneider M, Hoffmann H and Zweck J 2001 *Appl. Phys. Lett.* **79** 3113
[4] Guslienko K Yu, Novosad V, Otani Y, Shima H and Fukamichi K 2001 *Phys. Rev.* B **65** 024414
[5] Bader S D 2006 *Rev. Mod. Phys.* **78** 1
[6] Chien C L, Zhu F Q and Zhu J-G 2007 *Phys. Today* **92** 40
[7] Fu H and Bellaiche L 2003 *Phys. Rev. Lett.* **91** 257601
[8] Naumov I, Bellaiche L and Fu H 2004 *Nature* **432** 737
[9] Zhu X H, Evans P R, Byrne D, Schilling A, Douglas C, Pollard R J, Bowman R M, Gregg J M, Morrison F D and Scott J F 2006 *Appl. Phys. Lett.* **89** 122913
[10] Scott J F 2006 *J. Phys.: Condens. Matter* **18** R361
[11] Ponomareva I *et al* 2005 *Phys. Rev.* B **72** 140102(R)
Ponomareva I, Naumov I I and Bellaiche L 2005 *Phys. Rev.* B **72** 214118
[12] Naumov I and Fu H 2007 *Phys. Rev. Lett.* **98** 077603
[13] Prosandeev S, Ponomareva I, Kornev I, Naumov I and Bellaiche L 2006 *Phys. Rev. Lett.* **96** 237601
[14] Prosandeev S, Kornev I and Bellaiche L 2007 *Phys. Rev.* B **76** 012101
[15] Prosandeev S and Bellaiche L 2007 *Phys. Rev.* B **75** 094102
[16] Prosandeev S and Bellaiche L 2006 *Phys. Rev. Lett.* **97** 167601
[17] Prosandeev S, Ponomareva I, Kornev I and Bellaiche L 2008 *Phys. Rev. Lett.* **100** 047201
[18] Zhong W, Vanderbilt D and Rabe K M 1994 *Phys. Rev. Lett.* **73** 1861
Zhong W, Vanderbilt D and Rabe K M 1995 *Phys. Rev.* B **52** 6301
[19] Voigt W 1910 *Lehrbuch der Kristallphysik* (Leipzig: Teubner) (reprinted in 1928 with an additional appendix)
[20] Bellaiche L, García A and Vanderbilt D 2000 *Phys. Rev. Lett.* **84** 5427
Bellaiche L, García A and Vanderbilt D 2002 *Ferroelectrics* **266** 41
[21] Iniguez J and Vanderbilt D 2002 *Phys. Rev. Lett.* **89** 115503
[22] Almahmoud E, Navtsenya Y, Kornev I, Fu H and Bellaiche L 2004 *Phys. Rev.* B **70** 220102(R)
[23] Naumov I I and Fu H 2005 *Preprint* cond-mat/0505497
[24] García A and Vanderbilt D 1998 First-principles calculations for ferroelectrics *5th Williamsburg Workshop* ed R E Cohen (Woodbury, NY: AIP) p 54
[25] Fedorov I, Petzelt J, Zelezny V, Komandin G A, Volkov A A, Brooks K, Huang Y and Setter N 1995 *J. Phys.: Condens. Matter* **7** 4313
[26] Nakamura K, Ito T and Freeman A J 2003 *Phys. Rev.* B **68** 180404(R)
[27] Jaffe B, Cook W R and Jaffe H 1971 *Piezoelectric Ceramics* (London: Academic) p 136
[28] Kittel C 1946 *Phys. Rev.* **70** 965
[29] Stachiotti M G 2004 *Appl. Phys. Lett.* **84** 251
[30] Dubovik V M, Tosunyan L A and Tugushev V V 1986 *Zh. Eksp. Teor. Fiz.* **63** 344
[31] Dubovik V M and Tugushev V V 1990 *Phys. Rep.* **187** 145
[32] Dubovik V M and Cheshkov A A 1975 *Sov. J. Part. Nucl.* **5** 318
[33] Kahn A H and Layendeccker J 1964 *Phys. Rev.* **135** A1321
[34] Nye J F 1957 *Physical Properties of Crystals* (New York: Oxford University Press)
[35] Dubovik V M, Martsenyuk M A and Saha B 2000 *Phys. Rev.* E **61** 7087
[36] Grimmer H 1994 *Ferroelectrics* **161** 181
[37] Schmid H 2001 *Ferroelectrics* **252** 41
[38] Sirotin Yu I and Shaskolskaya M P 1979 *The Principles of Crystal Physics* (Moscow: Nauka)
[39] García A and Vanderbilt D 1998 *Appl. Phys. Lett.* **72** 2981
[40] Rabe K M and Cockayne E 1998 First-principles calculations for ferroelectrics *AIP Conf. Proc.* vol 436, ed R E Cohen (Woodbury, NY: American Institute of Physics)
[41] Caspari M E and Merz W J 1950 *Phys. Rev.* **80** 1082
[42] Hamilton J 2004 *A Life of Discovery: Michael Faraday, Giant of the Scientific Revolution* (New York: Random House)
[43] Bungaro C and Rabe K M 2002 *Phys. Rev.* B **65** 224106
[44] Guslienko K Yu 2001 *Appl. Phys. Lett.* **78** 3848
[45] Heyderman L J, Nolting F, Backes D, Czekaj S, Lopez-Diaz L, Kläui M, Rüdiger U, Vaz C A F, Bland J A C, Matelon R J, Volkmann U G and Fischer P 2006 *Phys. Rev.* B **73** 214429
[46] Eleftheriades G V, Iyer A K and Kremer P C 2002 *IEEE Trans. Microw. Theory Tech.* **50** 2702